ELSEVIER

Solid State Nuclear Magnetic Resonance 6 (1996) 73–83

SOLID STATE
Nuclear Magnetic
Resonance

Two-dimensional magic-angle spinning isotropic reconstruction sequences for quadrupolar nuclei

D. Massiot [a], B. Touzo [a], D. Trumeau [a], J.P. Coutures [a], J. Virlet [b], P. Florian [c], P.J. Grandinetti [c,*]

[a] *Centre de Recherches sur la Physique des Hautes Températures, 1D Ave de la Recherche Scientifique, 45071 Orléans Cedex 2, France*
[b] *Service de Chimie Moléculaire, Commissariat à l'Energie Atomique, C.E. Saclay, 91191 Gif-sur-Yvette Cedex, France*
[c] *Department of Chemistry, The Ohio State University, 120 W. 18th Avenue Columbus, OH 43210-1173, USA*

Received 17 July 1995; accepted 20 September 1995

Abstract

Two-dimensional magic-angle spinning (triple quantum, single quantum) correlation pulse sequences and phase cycles based on the technique of Frydman and Harwood for the reconstruction of the isotropic spectrum of half-integer spin quadrupolar nuclei broadened to second-order are described. These sequences provide pure absorption mode two-dimensional lineshapes and increased sensitivity. Experimental examples on spin $I = 3/2$ (^{87}Rb in $RbNO_3$) and $I = 5/2$ (^{27}Al in $NaSi_3AlO_8$) are presented. The isotropic chemical shift and quadrupolar coupling parameters could be obtained from a simple analysis of the triple quantum filtered single quantum magic-angle spinning cross-sections.

Keywords: Isotropic spectrum; Multiple quantum; Pure absorption mode lineshape; Quadrupolar nucleus

1. Introduction

The recent discovery by Frydman and Harwood [1] that an isotropic spectrum of a quadrupolar nucleus broadened to second-order can be obtained from a skew projection of a two-dimensional magic-angle spinning (MAS) (triple quantum, single quantum) correlation spectrum has opened up exciting new possibilities in solid-state NMR. The apparent difficulty in this new technique lies in the excitation of triple quantum coherences in a system where the first-order quadrupolar interaction dominates the rotating frame Hamiltonian. In the originally proposed two-dimensional MAS sequence of Frydman and Harwood [1] excitation of the triple quantum coherence was accomplished using two pulses separated by a time delay on the order of the inverse of the quadrupolar splitting. After free evolution as triple quantum coherence, this coherence was transferred into single quantum coherence with a single pulse.

In this paper we present two new two-dimensional MAS sequences based on the triple quantum excitation schemes of Vega and Naor [2] that replace the two-pulse triple quantum excitation sequence with a single pulse. In 1984 Vega and Naor [2] showed, in cases where the r.f. ampli-

* Corresponding author.

SSDI 0926-2040(95)01210-9

tude is weak with respect to the first-order quadrupolar interaction, that the triple quantum coherences can be more efficiently created or indirectly detected in spin 3/2 systems with a single radio frequency pulse. In addition, our new two-dimensional MAS sequences are designed to provide the two-dimensional correlation with pure absorption mode two-dimensional lineshapes. Pure absorption mode two-dimensional lineshapes facilitate the analysis of lineshapes in the anisotropic dimension to extract quadrupolar tensor information. Although this two-dimensional MAS experiment suffers from the constraint that not all crystallite orientations are uniformly excited, and thus the anisotropic lineshapes in the second dimension are distorted, our results suggest that in some situations those distortions are minimal and that this approach can be used to obtain quadrupolar tensor parameters.

Our first approach combines the two-pulse sequence of Vega and Naor with the traditional hypercomplex method to obtain phase separation. This two-pulse sequence was also recently used by Fernandez and Amoureux [3] to increase the sensitivity in the Frydman and Harwood experiment, however, in their application the hypercomplex approach to pure absorption mode spectra was not employed. Our second approach uses the shifted-echo method [4], recently developed for dynamic-angle spinning [5–17], to obtain phase separation. The shifted-echo method has the advantage of an additional $2^{1/2}$ improvement in signal-to-noise when compared to the hypercomplex or time proportional phase increment (TPPI) approach.

2. Pulse sequences

While Vega and Naor considered only the case of a single crystal, the case of a polycrystalline sample is considerably more complicated since there exists no single pulse length that excites all crystallites equally. In general, in the limit where the r.f. field strength, ω_1 is weak with respect to the orientation dependent first-order quadrupolar interaction, $\omega_Q A_{20}(\theta, \phi)$, the nutation frequency of an n-quantum coherence during a pulse is proportional to $\omega_1^n/[\omega_Q A_{20}(\theta, \phi)]^{n-1}$ [2,18,19], where θ and ϕ are the angles between the principal axis system of the quadrupolar interaction and the external magnetic field. Therefore, the optimal pulse length will depend on the relative orientations and size of the quadrupolar interactions, which of course, will be specific to the sample under consideration. In this paper we do not attempt to determine the pulse lengths for optimum sensitivity. We simply set the lengths of triple quantum excitation and detection pulses in both sequences to an integer multiple (typically 1–3 times) of the 2π pulse length for the central transition. This has the effect of reducing the single quantum coherence amplitude during t_1 evolution.

2.1. Hypercomplex sequence

The traditional approach for obtaining a pure absorption mode two-dimensional lineshape is to separate the signals arising from the echo and anti-echo pathways. This can be done using either TPPI or the hypercomplex approach. In this paper we will choose the latter. In the hypercomplex approach, two phase cycles are used to produce two signals that are linear combinations of the echo and anti-echo signal.

The two pulse sequence is shown in Fig. 1. For spin 5/2 the echo pathway is $p = 0 \rightarrow 3 \rightarrow -1$, while the anti-echo pathway is $p = 0 \rightarrow -3 \rightarrow -1$. For spin 3/2 these assignments are reversed. In the following discussion we will treat the spin 5/2 case. The treatment will apply equally as well to the spin 3/2 case keeping in mind the assignment reversal.

Selecting the echo and anti-echo pathway is accomplished using the pulse phase relationship [20]:

$$\phi_R = -3\phi_1 + 4\phi_2 \quad (1)$$

Assuming that the receiver detects only coherences at -1, we phase cycle the first pulse through increments of $\Delta\phi_1 = 360°/6$ to eliminate all the Δp_1 values in parentheses below:

$$\Delta p_1 = \cdots (-5), (-4), \mathbf{-3}, (-2), (-1), (0), (1), (2), \mathbf{3}, (4), (5), \cdots \quad (2)$$

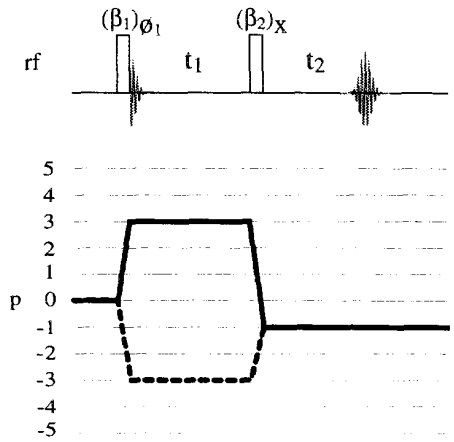

Fig. 1. Two-pulse magic-angle spinning isotropic reconstruction sequence for quadrupolar nuclei broadened to second-order. Pulse lengths β_1 and β_2 are set to an integer multiple (typically 1–3 times) of the 2π pulse length for the central transition in order to reduce the single quantum coherence amplitudes during t_1 evolution.

This leads to the phase cycle:

$\phi_1 = 0°$	60°	120°	180°	240°	300°
$\phi_2 = 0°$					
$\phi_R = 0°$	180°				

(3)

which generates the signal $S_X(t_1, t_2)$. $S_X(t_1, t_2)$ contains a linear combination of the echo and anti-echo signals. The echo and anti-echo signals can be separated by phase shifting the first pulse by $90°/|p|$, where p is the order of the coherence in the t_1 evolution period, in this case $|p| = 3$. This leads to the phase cycle:

$\phi_1 = 30°$	90°	150°	210°	270°	330°
$\phi_2 = 0°$					
$\phi_R = 0°$	180°				

(4)

which generates the signal $S_Y(t_1, t_2)$. From $S_X(t_1, t_2)$ and $S_Y(t_1, t_2)$ we construct the echo and anti-echo signals, $S_E(t_1, t_2)$ and $S_A(t_1, t_2)$ respectively, according to:

$$S_E(t_1, t_2) = S_X(t_1, t_2) - iS_Y(t_1, t_2) \quad (5)$$

$$S_A(t_1, t_2) = S_X(t_1, t_2) + iS_Y(t_1, t_2) \quad (6)$$

To eliminate the need for a skew projection a shearing transformation may be applied so that the isotropic spectrum can be obtained from a simple projection of the final 2D spectrum. This transformation can be implemented by applying a t_1-dependent first-order phase correction:

$$\begin{aligned} S'_E(t'_1, \omega'_2) &= e^{i\phi(t_1, \omega_2)} S_E(t_1, \omega_2) \\ S'_A(t'_1, \omega'_2) &= e^{-i\phi(t_1, \omega_2)} S_A(t_1, \omega_2) \end{aligned} \quad (7)$$

where

$$\phi(t_1, \omega_2) = k\omega_2 t_1 \quad (8)$$

prior to the final Fourier transform with respect to t'_1. Here $k = 7/9$ for the case of $I = 3/2$ and $k = 19/12$ for the case of $I = 5/2$ (see Appendix). After this phase correction the dwell time in t'_1 is increased from the t_1 dwell time by a factor of $k + 1$. Additional zero- and first-order phase corrections may be needed to phase the $t_1 = 0$ cross-section of both the echo and anti-echo signals into pure absorption mode real spectra. The pure absorption mode 2D spectrum $S(\omega'_1, \omega'_2)$ is then obtained by Fourier transforming $S'_E(t'_1, \omega'_2)$ and $S'_A(t'_1, \omega'_2)$ with respect to t'_1 and then combining according to

$$S(\omega'_1, \omega'_2) = S'_E(\omega'_1, \omega'_2) + S'_A(-\omega'_1, \omega'_2) \quad (9)$$

After the shearing transformation, the position of the resonances (in ppm) in the isotropic projection for the spin $I = 3/2$ case (see Appendix) is given by:

$$\omega^{(iso)} = \frac{17}{8}\Delta\sigma + \frac{1 \times 10^6}{8}\frac{\omega_Q^2}{\omega_0^2}\left(\frac{\eta^2}{3} + 1\right) \quad (10)$$

and for the spin $I = 5/2$ case (see Appendix) by:

$$\Omega^{iso} = -\frac{17}{31}\Delta\sigma - \frac{8 \times 10^6}{93}\frac{\omega_Q^2}{\omega_0^2}\left(\frac{\eta^2}{3} + 1\right) \quad (11)$$

where $\Delta\sigma$ is the difference between the isotropic chemical shift and the reference, $\omega_Q = 6\pi C_q/2I(2I-1)$, ω_0 is the Zeeman frequency, and C_q and η are the quadrupolar coupling pa-

rameters. If the spectrum is to be referenced to a frequency other than the r.f. carrier frequency (i.e. zero is not defined in the middle of the spectrum), then the reference offset used in the single quantum dimension must be multiplied by a factor of $(3+k)/(1+k)$ for the $I=3/2$ case and $(-3+k)/(1+k)$ for the $I=5/2$ case when used in the isotropic dimension.

2.2. Shifted echo sequence

Another approach to obtaining a pure absorption mode two-dimensional lineshape is the shifted-echo approach [4]. This approach was first applied to dynamic-angle spinning (DAS), and is limited to systems exhibiting significant inhomogeneous broadenings as are typically found in solid-state NMR. In the shifted echo approach we add an additional π pulse in the sequence to shift the coherence transfer echo into the t_2 evolution time so that we can obtain the whole echo for $t_1=0$. Using the time shift theorem, we can approximately extend the lower limit of the Fourier integral in t_2 to $-\infty$ and eliminate all dispersion-mode terms from our spectrum in t_2.

The shifted-echo pulse sequence is shown in Fig. 2. As in the previous section we define the echo pathway for spin 5/2 as $p=0\rightarrow 3\rightarrow 1\rightarrow -1$, while the anti-echo pathway is $p=0\rightarrow -3\rightarrow 1\rightarrow -1$. Again, for spin 3/2 these assignments are reversed. Selecting the echo pathway is accomplished using the pulse phase relationship:

$$\phi_R = -3\phi_1 + 2\phi_2 + 2\phi_3 \tag{12}$$

and selecting the following coherence transfers for the first and third pulse,

$$\begin{aligned}\Delta p_1 &= \cdots(-5),(-4),(-3),(-2),(-1),\\ &\quad (0),(1),(2),\mathbf{3},(4),(5),\cdots\\ \Delta p_3 &= \cdots(-6),(-5),(-4),(-3),\mathbf{-2},\\ &\quad (-1),(0),(1),(2),(3),(4),\cdots\end{aligned} \tag{13}$$

Cycling the first pulse phase through increments of $\Delta\phi_1 = 360°/12$ to eliminate all the Δp_1 values in parentheses above, and cycling the third pulse phase through increments of $\Delta\phi_3 = 360°/8$ to eliminate all the Δp_3 values in parentheses above leads to the echo phase cycle:

$\phi_1 = 0°$	30°	60°	90°	120°	150°	180°	210°	240°	270°	300°	330°
$\phi_2 = 0°$											
$\phi_3 = 0°$	0°	0°	0°	0°	0°	0°	0°	0°	0°	0°	0°
45°	45°	45°	45°	45°	45°	45°	45°	45°	45°	45°	45°
90°	90°	90°	90°	90°	90°	90°	90°	90°	90°	90°	90°
135°	135°	135°	135°	135°	135°	135°	135°	135°	135°	135°	135°
180°	180°	180°	180°	180°	180°	180°	180°	180°	180°	180°	180°
225°	225°	225°	225°	225°	225°	225°	225°	225°	225°	225°	225°
270°	270°	270°	270°	270°	270°	270°	270°	270°	270°	270°	270°
315°	315°	315°	315°	315°	315°	315°	315°	315°	315°	315°	315°
$\phi_R = 0°$	270°	180°	90°	0°	270°	180°	90°	0°	270°	180°	90°
90°	0°	270°	180°	90°	0°	270°	180°	90°	0°	270°	180°
180°	90°	0°	270°	180°	90°	0°	270°	180°	90°	0°	270°
270°	180°	90°	0°	270°	180°	90°	0°	270°	180°	90°	0°

(14)

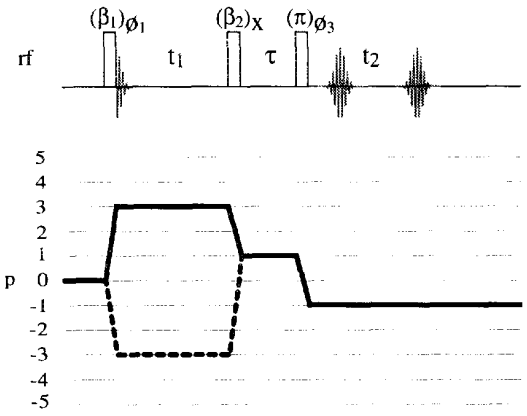

Fig. 2. Three-pulse shifted-echo magic-angle spinning isotropic reconstruction sequence for quadrupolar nuclei broadened to second-order. As in the two-pulse experiment the pulse lengths β_1 and β_2 are set to an integer multiple (typically 1–3 times) of the 2π pulse length for the central transition in order to reduce the single quantum coherence amplitudes during t_1 evolution. The last pulse is adjusted to be a selective π pulse on the central transition. The length of τ is a multiple of the rotor period, and typically half the width of the echo, so that the signal in t_2 begins at zero.

This phase cycle alone will provide pure absorption mode lineshapes for spin 5/2.

Selecting the anti-echo pathway is accomplished using the pulse phase relationship:

$$\phi_R = 3\phi_1 - 4\phi_2 + 2\phi_3 \tag{15}$$

and selecting the following coherence transfers for the first and third pulse,

$$\begin{aligned}\Delta p_1 = {} & \cdots(-5), (-4), \mathbf{-3}, (-2), (-1), (0),\\ & (1), (2), (3), (4), (5), \cdots\\ \Delta p_3 = {} & \cdots(-6), (-5), (-4), (-3), \mathbf{-2},\\ & (-1), (0), (1), (2), (3), (4), \cdots\end{aligned} \tag{16}$$

Cycling the first pulse phase through increments of $\Delta\phi_1 = 360°/12$ to eliminate all the Δp_1 values in parentheses above, and cycling the third pulse phase through increments of $\Delta\phi_3 = 360°/8$ to eliminate all the Δp_3 values in parentheses above leads to the anti-echo phase cycle:

$\phi_1 = 0°$	30°	60°	90°	120°	150°	180°	210°	240°	270°	300°	330°
$\phi_2 = 0°$											
$\phi_3 = 0°$	0°	0°	0°	0°	0°	0°	0°	0°	0°	0°	0°
45°	45°	45°	45°	45°	45°	45°	45°	45°	45°	45°	45°
90°	90°	90°	90°	90°	90°	90°	90°	90°	90°	90°	90°
135°	135°	135°	135°	135°	135°	135°	135°	135°	135°	135°	135°
180°	180°	180°	180°	180°	180°	180°	180°	180°	180°	180°	180°
225°	225°	225°	225°	225°	225°	225°	225°	225°	225°	225°	225°
270°	270°	270°	270°	270°	270°	270°	270°	270°	270°	270°	270°
315°	315°	315°	315°	315°	315°	315°	315°	315°	315°	315°	315°
$\phi_R = 0°$	90°	180°	270°	0°	90°	180°	270°	0°	90°	180°	270°
90°	180°	270°	0°	90°	180°	270°	0°	90°	180°	270°	0°
180°	270°	0°	90°	180°	270°	0°	90°	180°	270°	0°	90°
270°	0°	90°	180°	270°	0°	90°	180°	270°	0°	90°	180°

(17)

This phase cycle alone will provide pure absorption mode two-dimensional lineshapes for spin 3/2.

Just as in the case of hypercomplex shifted-echo DAS, there are certain situations where an additional factor of $2^{1/2}$ enhancement in the signal-to-noise ratio can be obtained by combining phase separation in t_1 with shifting the echo in t_2. As in the hypercomplex sequence of the previous section the echo and anti-echo phase cycles can be separated into halves. The first half generates a signal $S_X(t_1, t_2)$, which has the phase cycle:

$\phi_1 = 0°$	60°	120°	180°	240°	300°
$\phi_2 = 0°$					
$\phi_3 = 0°$	0°	0°	0°	0°	0°
45°	45°	45°	45°	45°	45°
90°	90°	90°	90°	90°	90°
135°	135°	135°	135°	135°	135°
180°	180°	180°	180°	180°	180°
225°	225°	225°	225°	225°	225°
270°	270°	270°	270°	270°	270°
315°	315°	315°	315°	315°	315°
$\phi_R = 0°$	180°	0°	180°	0°	180°
90°	270°	90°	270°	90°	270°
180°	0°	180°	0°	180°	0°
270°	90°	270°	90°	270°	90°

(18)

and the second half generates a signal $S_Y(t_1, t_2)$, which has the phase cycle:

$\phi_1 = 30°$	90°	150°	210°	270°	330°
$\phi_2 = 0°$					
$\phi_3 = 0°$	0°	0°	0°	0°	0°
45°	45°	45°	45°	45°	45°
90°	90°	90°	90°	90°	90°
135°	135°	135°	135°	135°	135°
180°	180°	180°	180°	180°	180°
225°	225°	225°	225°	225°	225°
270°	270°	270°	270°	270°	270°
315°	315°	315°	315°	315°	315°
$\phi_R = 0°$	180°	0°	180°	0°	180°
90°	270°	90°	270°	90°	270°
180°	0°	180°	0°	180°	0°
270°	90°	270°	90°	270°	90°

(19)

From $S_X(t_1, t_2)$ we construct $S_E(t_1, t_2)$ and $S_A(t_1, t_2)$ according to Eqs. (5) and (6).

The length of τ is a multiple of the rotor period, and typically half the width of the echo, so that the signal in t_2 begins at zero. The complex two-dimensional data acquired with this sequence are processed in the same fashion as in the last section, with the only difference being a τ-dependent first-order phase correction of

$$\phi(\tau, \omega_2) = \omega_2 \tau \tag{20}$$

to remove the phase modulation because of the time-shifted echo, and the t_1-dependent first-order correction of Eq. (8) to perform the shearing transformation. Both are applied after the Fourier transform with respect to t_2.

A potential difficulty with this approach is that τ must be adjusted to be large enough to obtain the whole echo signal. If the homogeneous broadenings, e.g. λ, are so large that

$$e^{-2\lambda\tau} \leq 1/2^{1/2} \tag{21}$$

then the hypercomplex sequence of Fig. 1 should be the preferred approach. Truncating the echo on either side of its maximum will add dispersion-mode components into the 2D spectrum. In practice, however, some truncation of the echo tail can be tolerated since this distortion is often no worse than the distortions obtained from acquisition dead times in the sequence of Fig. 1.

Before the shearing transformation the Zeeman and chemical shift offsets from the carrier frequency during t_1 of all triple quantum coherences are shifted away from zero by a factor of three. Therefore, even if the triple quantum spectrum is bandwidth limited to approximately the same width as the single quantum spectrum, there may be aliasing of resonances in ω_1 if the spectral width used in t_2 is also used in t_1. One expensive solution to this problem is to use a shorter dwell time in t_1, because this results in unnecessarily longer experiments. A simple solution is to use the minimum spectral width in t_1 needed for the triple quantum spectrum bandwidth, and then apply a first-order phase correction to the t_1 time-domain to shift the triple quantum spectrum back into the spectral width. A related approach is to employ TPPI[21] to the first pulse in the sequence to shift the triple quantum resonances back into the spectral width. That is, shift all the phases of the first pulse in the sequence by $\Delta\Omega t_1/3$, where $\Delta\Omega$ is the shift needed to move the resonances back into the spectral width.

3. Experimental

$RbNO_3$ was obtained commercially, kept in a dry atmosphere, and used without further purification. The natural albite sample, $NaSi_3AlO_8$, was characterized by X-ray diffraction and is of Amelia type (JCPDS 20-554). ^{87}Rb spectra were referenced relative to aqueous 1M $RbNO_3$ as an external frequency standard. ^{27}Al spectra were referenced relative to aqueous 1M $Al(NO_3)_3$ as an external frequency standard. All experiments were performed on a Bruker MSL spectrometer with a 7 T magnet and a commercial MAS (5 mm rotor) probe. Spinning speeds were typically between 10 and 12 kHz.

For the two-pulse ^{87}Rb experiment on $RbNO_3$ a 32 μs increment was used for both t_1 and t_2 with 240×256 hypercomplex $t_1 \times t_2$ points. Both dimensions were zero-filled to 512 points. For the two-pulse ^{27}Al experiment on $NaSi_3AlO_8$ a 60 μs increment was used for both t_1 and t_2 with 128×256 hypercomplex $t_1 \times t_2$ points. The t_1 dimension was zero-filled to 256 points.

For the three-pulse ^{87}Rb experiment on $RbNO_3$ an 80 μs increment was used in t_1, and a 60 μs increment was used in t_2 with 105×256 hypercomplex $t_1 \times t_2$ points. The t_1 dimension was zero-filled to 256 points. For the three-pulse ^{27}Al experiment on $NaSi_3AlO_8$ an 60 μs increment was used in both t_1 and t_2 with 128×256 hypercomplex $t_1 \times t_2$ points (spectrum not shown). The t_1 dimension was zero-filled to 256 points.

In all experiments the pulse duration of the triple quantum excitation and detection pulses, β_1 and β_2, were identical and were taken as the liquid π duration (typically 4–5 μs), which gave a good signal with minimum contribution of signal quantum coherences during t_1. In the shifted echo experiments the last pulse was adjusted to be a selective π pulse on the central transition. The length of τ was a multiple of the rotor

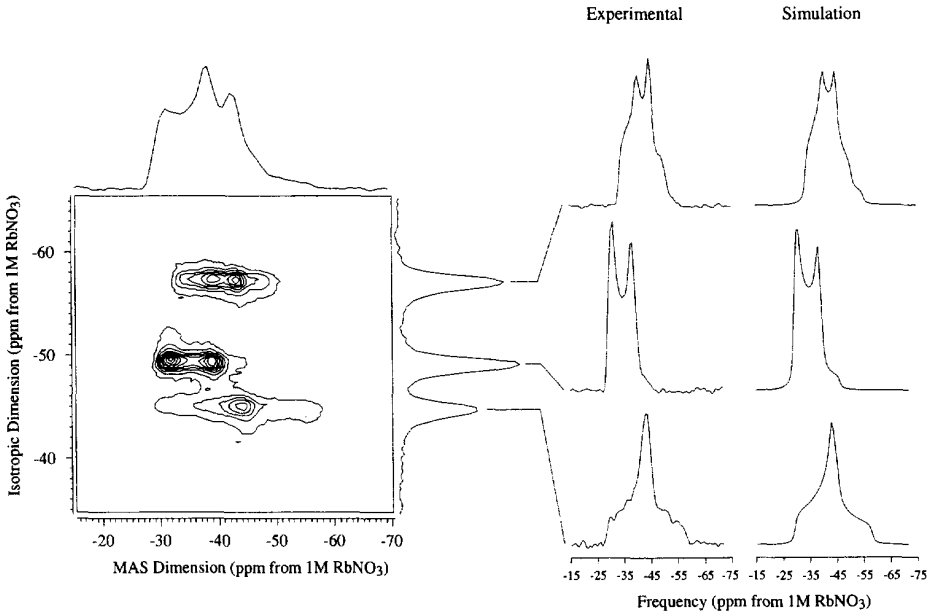

Fig. 3. On the left is the two-dimensional shifted echo (triple quantum, single quantum) ^{87}Rb MAS spectrum of $RbNO_3$ after shearing. The contour lines are drawn every 5% starting at a level of 5% and ending at 95% of the maximum point in the spectrum. On the right are the triple quantum filtered single quantum MAS cross-sections for each of the three crystallographically distinct sites in $RbNO_3$ along with "best fit" simulations.

Table 1
Comparison of ^{87}Rb NMR parameters of $RbNO_3$, obtained by fitting the triple quantum filtered single quantum MAS cross-section lineshapes, with magic-angle detected dynamic-angle spinning experiments

Site	This work				Ref. [12]		
	δ_{iso}^{obs}(ppm)	δ_{iso}^{cs}(ppm)	C_q(MHz)	η	δ_{iso}^{cs}(ppm)	C_q(MHz)	η
1	−49.0	−27.4	1.68	0.2	−26.2	1.83	0.12
2	−44.7	−28.5	1.94	1.0	−26.8	2.07	1.0
3	−57.1	−31.3	1.72	0.5	−30.9	1.85	0.48

period, and typically half the width of the echo, so that the signal in t_2 begins at zero.

All spectra were processed according to the same procedures described for DAS[4]. For hypercomplex processing, the echo and anti-echo 2D signals were obtained from the hyper-complex data using Eqs. (5) and (6). Both the echo and anti-echo signals are processed in parallel before combining the final two-dimensional Fourier transforms as described by Eq. (9). Prior to Fourier transforming, the two-dimensional time domain data are apodized with a shifted Gaussian that follows the echo tops. After Fourier transforming with respect to t_2, a shearing transformation using the t_1-dependent phase of Eq. (8) is applied, in addition to the usual zero- and first-order phase correction needed to phase the $t_1 = 0$ spectra of both the echo and anti-echo spectra into pure absorption mode. In the case of the shifted-echo experiment the final Fourier transform with respect to t_1' gives the pure absorption mode two-dimensional spectrum. In the case of the hypercomplex experiment after the final Fourier transform with respect to t_1' for both the echo and anti-echo spectra, the anti-echo two-dimensional spectrum is reversed in the ω_1'

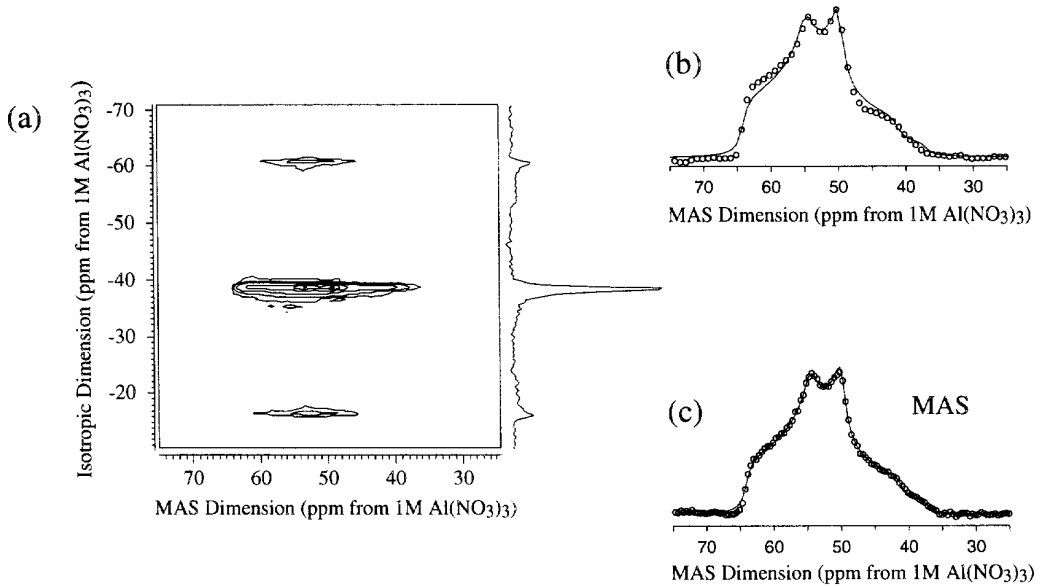

Fig. 4. (a) The two-dimensional hypercomplex (triple quantum, single quantum) ^{27}Al MAS spectrum of $NaSi_3AlO_8$ after shearing. The contour lines are drawn at levels of 5, 10, 20, 50, 80 and −95% of the maximum point in the spectrum. (b) The triple quantum filtered single quantum MAS cross-section for $NaSi_3AlO_8$ along with "best fit" simulation. (c) The one-pulse single quantum MAS spectrum along with "best fit" simulation. Other than some minor distortion in the extreme shoulders, the spectrum in (b) is remarkably similar to (c).

dimension and added to the echo two-dimensional spectrum to obtain the pure absorption mode two-dimensional spectrum.

Anisotropic lineshapes were fit using a least squares procedure [22,23] to obtain the quadrupolar and chemical shift parameters.

4. Results

As an example of a spin $I = 3/2$ case we have used ^{87}Rb in $RbNO_3$. On the left in Fig. 3 is the pure absorption mode (triple quantum, single quantum) shifted-echo two-dimensional MAS spectrum of $RbNO_3$ after shearing. $RbNO_3$ has three crystallographically distinct sites [24] that are all resolved in the isotropic dimension. The integrated intensities of all three peaks in 19:14:17 in close agreement with the 1:1:1 ratio obtained from the crystallographic structure. On the right in Fig. 3 are the triple quantum filtered single quantum MAS cross-sections for each of the three crystallographically distinct sites in $RbNO_3$ along with "best fit" simulations, obtained using the fitting constraint of the observed isotropic position given by Eq. (10). One might have expected strong distortions in the anisotropic lineshapes due to the triple quantum filtering. However, the lineshapes in these cross-sections are remarkably close to the expected anisotropic lineshapes assuming equal excitation of all crystallite orientations. Other than some minor baseline distortions due to receiver deadtime, identical lineshapes are obtained with the two-pulse hypercomplex sequence (spectrum not shown). The "best fit" parameters obtained from the anisotropic lineshapes using the isotropic position as an additional constraint are given in Table 1 along with the previously obtained parameters using magic-angle detected dynamic-angle spinning experiments [12].

As an example of a spin $I = 5/2$ case we have used ^{27}Al in $NaSi_3AlO_8$. Fig. 4 shows the two-dimensional pure absorption mode (triple quantum, single quantum) MAS spectrum of albite after heating. Other than a minor distortion of the extreme shoulders, the triple quantum filtered single quantum MAS cross-section is remarkably similar to the simple one-pulse MAS spectrum also shown in Fig. 4. Similar NMR parameters are obtained from fitting these lineshapes, and are given in Table 2.

5. Summary

Based on the isotropic reconstruction experiment of Frydman and Harwood we have devised two new approaches for obtaining pure absorption mode two-dimensional (triple quantum, single quantum) correlation spectra of second-order broadened quadrupolar nuclei.

Combining the two-pulse triple quantum excitation and detection sequence of Vega and Naor with the traditional hypercomplex approach and a shearing transformation we obtain a pure absorption mode two-dimensional correlation between the isotropic site-resolved spectrum and the triple quantum filtered ^{87}Rb MAS spectrum for the three sites of $RbNO_3$. Application of this technique to the ^{27}Al resonance in albite is also demonstrated. In a second sequence we use the shifted echo approach of DAS and add an additional π-pulse after the two-pulse triple quantum evolution in order to time shift the coherence transfer echoes into the t_2 acquisition window to obtain whole echo acquisition, and thus a pure absorption mode two-dimensional spectrum with a $\sqrt{2}$ improvement in sensitivity. Application of this technique is also demonstrated on ^{87}Rb in $RbNO_3$.

Table 2
^{27}Al NMR parameters of $NaSi_3AlO_8$ obtained by fitting the triple quantum filtered single quantum MAS cross-section lineshapes

Technique	δ_{iso}^{obs}(ppm)	δ_{iso}^{cs}(ppm)	C_q(MHz)	η
MAS	—	64.5	3.22	0.66
3Q filtered MAS	−38.4	64.7	3.25	0.68

In all cases we were able to obtain triple quantum filtered MAS lineshapes that were remarkably close to simple one-pulse MAS lineshapes where all crystallites are excited equally.

Acknowledgments

This work was supported in part by the National Science Foundation, through grant No. CHE-9501872 to P.J.G. D.M., B.T., D.T. and J.P.C. thank the CNRS (UP4212) and Region Centre for financial support.

Appendix A. Calculation of isotropic shifts

The time averaged second-order quadrupolar ($m \rightarrow -m$ transition) NMR frequency of a coherence of order $p = 2m$ while spinning at an angle β with respect to the external magnetic field is given by:

$$\Omega_p = -\frac{\omega_Q^2}{\omega_0} \sum_{L=0,2,4} C_L^I(p) P_L(\cos\beta) \sqrt{\frac{4\pi}{2L+1}} \times \sum_{n=-L}^{L} \sigma_{Ln} Y_{Ln}(\theta, \phi) \quad \text{(A1)}$$

where

$$C_L^I(p) = 2p \sum_{k=1,2} \frac{\langle L\ 0 \mid 2\ 2\ k-k \rangle}{k} \times \left[I(I+1) - \frac{p^2}{2k} - \frac{k}{4} \right] \quad \text{(A2)}$$

$P_L(x)$ is the Lth rank Legendre polynomial,

$$\sigma_{Ln} = \sum_{k=0,2,4} \langle L\ n \mid 2\ 2\ k\ n-k \rangle \rho_{2k} \rho_{2n-k} \quad \text{(A3)}$$

where $\rho_{20} = 1/\sqrt{6}$, $\rho_{2\pm2} = \eta/6$, $\langle L\ m \mid l_1\ l_2\ m_1\ m_2 \rangle$ is the Clebsch–Gordon coefficient, and $Y_{Ln}(\theta, \phi)$ is the spherical harmonic, where θ and ϕ are the angles between the principal axis system of the quadrupolar interaction and the rotor frame. Values for the coefficients $C_L^I(p)$ are given in Table A1.

In the experiment of Frydman and Harwood [1] the isotropic frequency will be the weighted average of the two frequencies. The weights are determined by the ratio of the $C_4^I(p)$ coefficients. This insures that the average fourth-rank anisotropic frequencies are all zero. Similar to DAS [9] we define $k = |C_4^I(\pm3)/C_4^I(-1)|$ so

$$\Omega^{(iso)} = \frac{1}{k+1}\Omega_{\pm3}^{(iso)} + \frac{k}{k+1}\Omega_{-1}^{(iso)} \quad \text{(A4)}$$

Next we can substitute the isotropic chemical shifts and quadrupolar second-order isotropic shifts associated with the two transitions. The single quantum (central transition $p = -1$ coherence) frequency (in ppm) is given by:

$$\Omega_{-1}^{(iso)} = \Delta\sigma - \frac{\omega_Q^2 \times 10^6}{\omega_0^2} C_0^I(-1)\sigma_{00} \quad \text{(A5)}$$

where $\Delta\sigma = \sigma_{iso} - \sigma_{ref}$ and $\sigma_{00} = (1/6\sqrt{5})((\eta^2/3) + 1)$. The triple quantum ($p = \pm3$ coherence) transition frequency (in ppm) is given by:

$$\Omega_{\pm3}^{(iso)} = \mp 3\Delta\sigma - \frac{\omega_Q^2 \times 10^6}{\omega_0^2} C_0^I(\pm3)\sigma_{00} \quad \text{(A6)}$$

Therefore for $I = 3/2$, where $k = 7/9$, using the $p = 0 \rightarrow -3 \rightarrow -1$ pathway the two-dimensional MAS isotropic frequency (in ppm) is:

$$\Omega^{(iso)} = \frac{9}{16} \times \Omega_{-3}^{(iso)} + \frac{7}{16} \times \Omega_{-1}^{(iso)} \quad \text{(A7)}$$

$$\Omega^{(iso)} = \frac{17}{8}\Delta\sigma + \frac{1 \times 10^6}{8} \frac{\omega_Q^2}{\omega_0^2} \left(\frac{\eta^2}{3} + 1 \right) \quad \text{(A8)}$$

Table A1
Spin and transition dependent part of the second-order quadrupolar NMR frequency

Coefft.	$I = 3/2$		$I = 5/2$		
	$p = 1$	$p = 3$	$p = 1$	$p = 3$	$p = 5$
$C_0^I(p)$	$-3/\sqrt{5}$	$9/\sqrt{5}$	$-8/\sqrt{5}$	$-6/\sqrt{5}$	$50/\sqrt{5}$
$C_2^I(p)$	$12/\sqrt{14}$	-0	$32/\sqrt{14}$	$60/\sqrt{14}$	$-20/\sqrt{14}$
$C_4^I(p)$	$27/\sqrt{70}$	$-21/\sqrt{70}$	$72/\sqrt{70}$	$114/\sqrt{70}$	$-150/\sqrt{70}$

Changing the sign of the coherence level also changes the sign of the coefficient.

and for $I = 5/2$, where $k = 19/12$, using the $p = 0 \rightarrow +3 \rightarrow -1$ pathway the two-dimensional MAS isotropic frequency (in ppm) is:

$$\Omega^{(iso)} = \frac{12}{31} \times \Omega_3^{(iso)} + \frac{19}{31} \times \Omega_{-1}^{(iso)} \quad \text{(A9)}$$

$$\Omega^{(iso)} = -\frac{17}{31}\Delta\sigma - \frac{8 \times 10^6}{93} \frac{\omega_Q^2}{\omega_0^2} \left(\frac{\eta^2}{3} + 1 \right) \quad \text{(A10)}$$

References

[1] L. Frydman and J.S. Harwood, J. Am. Chem. Soc., 117 (1995) 5367.
[2] S. Vega and Y. Naor, J. Chem. Phys., 75 (1981) 75.
[3] C. Fernandez and J.P. Amoureux, Solid State NMR, in press, 1995.
[4] P.J. Grandinetti, J.H. Baltisberger, A. Llor, Y.K. Lee, U. Werner, M.A. Eastman and A. Pines, J. Magn. Reson. A, 103 (1993) 72.
[5] A. Samoson, E. Lippmaa and A. Pines, Mol. Phys., 65 (1988) 1013.
[6] A. Llor and J. Virlet, Chem. Phys. Lett., 152 (1988) 248.
[7] B.F. Chmelka, K.T. Mueller, A. Pines, J. Stebbins, Y. Wu and J.W. Zwanziger, Nature, 339 (1989) 42.
[8] A. Samoson, B.Q. Sun and A. Pines, New angles in motional averaging, in D.M.S. Bagguley (Ed.), Pulsed Magnetic Resonance: NMR, ESR, and Optics — A recognition of E.L. Hahn, Clarendon Press, Oxford, 1992.
[9] K.T. Mueller, B.Q. Sun, G.C. Chingas, J.W. Zwanziger, T. Terao and A. Pines, J. Magn. Reson., 86 (1990) 470.
[10] K.T. Mueller, Y. Wu, B.F. Chmelka, J. Stebbins and A. Pines, J. Am. Chem. Soc., 113 (1991) 32.
[11] K.T. Mueller, J.H. Baltisberger, E.W. Wooten and A. Pines, J. Phys. Chem., 96 (1992) 7001.
[12] J.H. Baltisberger, S.L. Gann, E.W. Wooten, T.H. Chang, K.T. Mueller and A. Pines, J. Am. Chem. Soc., 114 (1992) 7489.
[13] M.A. Eastman, P.J. Grandinetti, Y.K. Lee and A. Pines, J. Magn. Reson., 98 (1992) 333.
[14] K.T. Mueller, E.W. Wooten and A. Pines, J. Magn. Reson., 92 (1990) 620.
[15] K.T. Mueller, G.C. Chingas and A. Pines, Rev. Sci. Instrum., 62 (1991) 1445.
[16] P.J. Grandinetti, Y.K. Lee, J.H. Baltisberger, B.Q. Sun and A. Pines, J. Magn. Reson. A, 102 (1993) 195.
[17] P.J. Grandinetti, Dynamic-angle spinning and applications, in D.M. Grant and R.K. Harris (Eds.), Encyclopedia of Nuclear Magnetic Resonance, John Wiley & Sons, New York, 1995.
[18] A. Wokaun and R.R. Ernst, J. Chem. Phys., 67 (1977) 1752.
[19] S. Vega, J. Chem. Phys., 68 (1978) 5518.
[20] R.R. Ernst, G. Bodenhausen and A. Wokaun, Principles of Nuclear Magnetic Resonance in One and Two Dimensions, Oxford University Press, Oxford, 1987.
[21] G. Drobny, A Pines, S. Sinton, D.P. Weitekamp and D. Wemmer, Symp. Faraday Soc., 13 (1980) 93.
[22] D. Massiot, H. Thiele and A. Germanus, Bruker Report, 140 (1994) 43.
[23] D. Massiot, D. Müller, T. Hubert, M. Schneider, A.P.M. Kentgens, B. Cote, J.P. Coutures and W. Gessner, Solid State NMR, 5 (1995) 175.
[24] C. Dean, T.W. Hambley and M.R. Snow, Acta Crystallogr. Sect. C, 40 (1984) 1512.